# Tailoring the chemical composition of LiMPO4 (M = Mg, Co, Ni) orthophosphates to design new inorganic pigments frommagenta to yellow Hue

Béatrice Serment, Lou Corucho, Alain Demourgues, Georges Hadziioannou, Cyril Brochon, Eric Cloutet, Manuel Gaudon

# Tailoring the chemical composition of $LiMPO_4$ (M=Mg, Co, Ni) orthophosphates to design new inorganic pigments from magenta to yellow hue

*Beatrice Serment*[†‡], *Lou Corucho*[†], *Alain Demourgues*[†], *Georges Hadziioannou*[‡], *Cyril Brochon*[‡], *Eric Cloutet*[‡], *and Manuel Gaudon*[†#]

[†] Institut de Chimie de la Matière Condensée de Bordeaux, UMR 5026 CNRS, 87 Avenue du Dr. Schweitzer,33608 Pessac Cedex, France

[‡] Laboratoire de Chimie des Polymères Organiques, LCPO, UMR 5629 CNRS,16 Avenue Pey-Berlan, 33607 Pessac Cedex, France

**ABSTRACT**

New inorganic pigments with intense and saturated colorations have been prepared by solid state route and exhibit a large color scale from magenta to yellow. Indeed, yellow and magenta are two of the three subtractive model's colors with wide application in printing or displays as e-book readers. To develop yellow and magenta hue, we focused on cobalt and nickel-based orthophosphates thanks to chemical stability, low density, low price and easy-preparation of such pigment class. All these orthophosphates crystallize with the well-known olivine-type structure (Pnma orthorhombic space group) where transition metals are stabilized in a distorted octahedral site. This paper deals with the optical absorption properties of various orthophosphates, the correlations with structural features and their colorimetric parameters (in L*a*b* color space). The $LiCo_{1-x}Mg_xPO_4$ series show near-magenta color with tunable luminosity while $LiNiPO_4$ compound exhibits a frank yellow coloration. $Co^{2+}$ ($^4T_1$) and $Ni^{2+}$ ($^4A_2$) chromophore ions occupy a more or less distorted octahedral site, leading to tune the intensity of d-d electronic transitions in the visible and NIR range and provide a

substractive color scale, i.e. $LiCo_{1-x}Ni_xPO_4$ solid solution possesses a very-rich panel of colors in between the two yellow and magenta extremes. It is worth noting that the crystal field splitting and B Racah parameter have been estimated in a first approximation on the basis of Tanabe-Sugano diagram and lead to conclude to a slightly higher crystal field splitting around 0.9 eV for $Ni^{2+}$ions and similar β covalent parameters, despite the same crystallographic sites of both these transition metals.

## 1. INTRODUCTION

Inorganic phosphates have attracted widespread attention in recent years for their potential applications as catalysts [1]–[3], ion exchange materials [4]–[6], optical components [7], [8], electrode materials for batteries [9], [10], and also as pigments [11], [12]. Inorganic pigments could be used as "core" for application such as inks due to their high hiding power and high refractive index which leads to a good screen contrast. Moreover, coloured compounds have been obtained by doping with chromophores cations or by using the antagonist link effect. Indeed, the diverse physicochemical properties of phosphates are directly or indirectly associated to the P-O bond covalence in the tetrahedral $PO_4^{3-}$ group; it can bind a wide range of structural units. Depending on the number of linked tetrahedral, phosphate anions are classified into orthophosphate, pyrophosphates and polyphosphates groups [13]. Moreover, among the inorganic compounds, the phosphate-based networks show some advantages as thermal and chemical stability (high oxidation resistance, low solubility) due to the high P-O bond covalency and so the refractory behaviour of the phosphate-based skeleton [14], [11]. Furthermore, phosphates have a high capacity to form solid solution and to stabilize various transition metals which induce various coloration [15]–[19]. For instance, $Co_3(PO_4)_2$ which exhibit a strong violet coloration, crystallizes in monoclinic symmetry ($P2_1/n$ space group) as $Mg_3(PO_4)_2$ with two $Co^{2+}$ ($3d^7$) sites, 5-fold coordinated to oxygen corresponding to a

distorted trigonal bipyramid and the other one to a distorted octahedron. $FePO_4$ phosphate which adopts several allotropic forms such as the berlinite structure of $AlPO_4$ (hexagonal symmetry with P321 space group) with $Fe^{3+}$ ($3d^5$) ions in a tetrahedral site, associated to dull-yellow color or the olivine network (orthorhombic symmetry with Pnma space group) with two crystallographic sites for $Fe^{3+}$ corresponding to distorted octahedral sites. The wide range of colours for these pigments is due to various 3d transition metals adopting centrosymmetric but mainly acentric sites inducing strong hue with high oscillator strength associated to the probability of electronic transitions.

In inorganic pigment field, three of the most interesting colours are cyan, magenta and yellow because they can be used in the inks industry as the three primary colours in devices/displays relying on colour subtractive addition. In colour printing, for illustration, the usual primary colours are cyan, magenta and yellow (CMY system). Cyan is the complement of red, magenta is the complement of green, and yellow the complement of blue. Combinations of different amounts of the three hue can produce a wide range of colours with strong saturation. Some applications, like the Elecphoretic Inks Displays (EPID) used this kind of colours, because the image is observed thanks to the reflection of light. [20]–[22]. The current challenge is to create coloured and highly charged inks in non-polar media. In fact, e-books readers are in grey scale or in colour due to the use of colour-filter with white/black EPD [23], [24]. A large claim that has trained recent developments is now for the synthesis of coloured electrophoretic inks [25]–[27]. The drawbacks of inorganic pigments are their high density which induced rapid sedimentation in non-polar media. Also, one additional advantage of phosphate compounds is their relatively low density issued from the light and covalent [$PO_4$] skeleton.

Magenta and yellow inorganic pigments have not been largely investigated with the objective to disperse them in organic media. Magenta pigments are mentioned in borates series [28],

whereas most of inorganic pigments detailed in literature are pink pigments, relatively far, in term of colorimetric parameters, from a magenta hue [29]–[31]. Besides the purple colour of $Co_3(PO_4)_2$, new purple-blue ceramic pigments corresponding to $CoZr_4(PO_4)_6$ and $CoKZr_2(PO_4)_3$ phosphates were recently investigated [32], [33], [34]. These frameworks derive from the NASICON-type structure [10] $NaZr_2(PO_4)_3$ where $Na^+$ ions occupy a regular octahedral site. These works showed that $Co^{2+}$ ion in octahedral coordination stabilized in phosphate network lead to purple coloration.

Regarding yellow pigments, the incorporation of $V^{5+}$ ($3d^0$) in $Y_2Ti_2O_7$ pyrochlore-phase with the generation of defects have been investigated [35]. In phosphate groups, $V^{5+}$-doped $BiPO_4$ has been recently investigated as new yellow pigments with high NIR reflectance [14]. With the goal of preparing ecologically and environmentally friendly specific pigments, the yellow–green pigment that consists of nontoxic elements was obtained by doping calcium ions into the cerium orthophosphate lattice Ca-doped $CePO_4$ solid solution [36]. In this phosphate, cerium ions adopt mixed valence states (3+, 4+) and are stabilized in a 9-fold coordination site. Tetravalent cerium stabilized in a dodecahedron site in perovskite network such as $Na_{0.66}Ce_{0.33}TiO_3$, recently discovered in our group, leads to a strong yellow coloration due to 2p(O)→ 4f(Ce) charge transfer band in visible range. Finally, it has to be cited the previous work on Ni-doped $SrZnP_2O_7$ diphosphate compounds, prepared by a conventional ceramic route, for which a frank yellow-orange colour has been obtained thanks to intra-atomic transitions of the $Ni^{2+}$ chromophore cations [37]. In this network, $Ni^{2+}$($3d^8$) is pentahedral coordinated to oxygens.

The paper is focused on the elaboration of cobalt or nickel phosphate pigments from solid state route with the target to develop a new generation of magenta and yellow pigments, respectively. Then on the basis of chemical composition and structural features, the optical absorption properties in UV-Visible-NIR range are deeply discussed. Phase purity has been

investigated using XRD analysis and unit-cell parameters have been extracted from full pattern matching. Experimental colorimetric parameters (in L*a*b* color-space) have been calculated from diffuse reflectance spectra and spectroscopic transitions have been attributed by considering the Tanabe-Sugano diagrams. Finally, the pigment tinting strength has been evaluated and discussed in regard of their incorporation in e-book inks.

## 2. EXPERIMENTAL PART

### *2.1 Synthesis*

$Co_3(PO_4)_2$, $NaCoPO_4$ and $LiCoPO_4$ and $LiCo_xM_{1-x}PO_4$ (M= Mg, Fe, Cu, Ni, Mn) powders were prepared by solid-state reaction from mixtures of $Li_2CO_3$, $Co(CH_3COO)$, $(NH_4)_2HPO_4$ and M metal acetate in stoichiometric proportions. Thermal treatments were performed in air atmosphere. A first step was carried out at 200°C during 12 h in order to decompose ammonium phosphate and start to eliminate the volatile species. The mixture was placed in alumina crucible protected with aluminum foil. Successive annealing with regrinding at 400°C in order to eliminate most of the organics (carbonates, ammonia) are required. All pigments were finally annealed at 900°C during 10 h. Cooling down to room temperature was slowly done at 1°C/min in the typical process, at the exception of the preparation of the β-$NaCoPO_4$ phase for which a rapid quenching under air is used.

### *2.2 Powder X-ray diffraction*

X-Ray diffraction (XRD) measurements were carried out on a PANalytical X'PERT PRO diffractometer equipped with an X-celerator detector, using Cu($K\alpha_1/K\alpha_2$) radiation. The spectra were recorded on 5-120° 2θ range with a time per step chosen in order to get at least 10,000 cps in intensity for the main diffractogram peak. The unit-cell parameters were accurately refined by full pattern matching on the diffractograms using Fullprof® program package [38]. The peak profiles are fitted with the Caglioti function, *i.e.* considering isotropic

crystallites. Uncertainties can be calculated from the standard deviation proposed by the software.

### *2.3 Diffuse reflectance measurements*

UV-Vis-NIR diffuse reflectance spectra were recorded at room temperature from 200 to 2500 nm with a step of 1 nm and a band length of 2 nm on a Cary 17 spectrophotometer using an integration sphere. Halon polymer was used as white reference for the blank. Optical properties are mainly presented after Kubelka-Munk transformation of the reflectance signal to emphasize the absorption bands: K/S (K-M transform) = $(1-R)^2/2R$, with R the reflectance of the powder bed. A mathematic treatment of the obtained spectra allowed the determination of the L*a*b* space colorimetric parameters, with-L* the luminosity, a* the green to red axis and b* the blue to yellow axis. The first step of the treatment consists in obtaining the XYZ tri-stimulus values (defined by the CIE, 1964) from the integration (on the visible range, i.e. from $\lambda$ = 380 nm up to 780 nm) of the product of $x(\lambda)$, $y(\lambda)$ or $z(\lambda)$ functions (CIE – 1964) with the diffuse reflectance spectra function: $X = \int x(\lambda).\ R(\lambda)d\ \lambda$. Then, the transfer equations defined by the CIE, 1976, from XYZ space to the L*a*b* space, were used in order to obtain the L*a*b* chromatic parameters.

## 3. RESULTS AND DISCUSSION

### *3.1. Preliminary results on $Co_3(PO_4)_2$, $NaCoPO_4$ and $LiCoPO_4$.*

With the aim to tend to the most beautiful magenta hue, $Co_3(PO_4)_2$, $NaCoPO_4$ and $LiCoPO_4$ phosphates were synthesized to compare their coloration. Here it can be defined, that a magenta is a pigment with L*a*b* parameters such as the luminosity L* is in the range 50-70, the red/blue ratio a*/b* about 3/-2 with the highest a* as possible (best organic pigment for inkjet can exhibit a* over 60). As far as we know, the colorimetric parameters of these three

cobalt-phosphates are not directly compared and discussed in literature, but independently studied [33], [39], [40]. Especially, $LiMPO_4$ have been investigating for their interesting pigment properties because a wide range of colors can be obtained when they are doped with one or more different transition metals (V, Cr, Mn, Fe, Co, Ni, Cu) [28], [41]. The solid state preparations have been carried out using same synthesis conditions at the exception of the cooling ramp of the thermal treatment which was varied for the preparation of β-$NaCoPO_4$. Their phase purity (XRD analyses) and their optical properties (UV-Vis-NIR absorption spectra in Kubelka-Munk (K-M) coordinates as well as their L*a*b* colorimetric parameters) are reported in **Figure 1**. $Co_3(PO_4)_2$ and $LiCoPO_4$ are shown to be obtained as pure single phase with $P2_1/c$ and Pnma space group, respectively.

For $NaCoPO_4$ composition, two allotropic varieties can be obtained depending on the cooling rate: the α-form corresponding to olivine structure with Pnma space group, *i.e.* isostructural to the $LiCoPO_4$ is obtained while a slow cooling down ramp is used; the β-form with $P2_1/n$ space group is obtained while a rapid quenching is performed. Hence, three different crystallographic forms can be obtained, with as main difference to take into account besides the cobalt-phosphate color, the coordination number of the chromophore cation ($Co^{2+}$). In $Co_3(PO_4)_2$ cobalt is distributed in both 5-fold coordinated and 6-fold coordinated site; in $MCoPO_4$ (M = Na or Li) alkaline cobalt phosphate with Pnma space group, cobalt ions are inserted in distorted octahedral site; in the β–$NaCoPO_4$ alkaline cobalt phosphate with $P2_1/n$ space group, cobalt ions are inserted in tetrahedral site. Thus, crystal field splitting around the chromophore is very different depending on the crystallographic structure. As it can be expected, for the preparation of purple/magenta colours, the cobalt has to be located in octahedral site. The β-$NaCoPO_4$ compound is blue-colored; the $Co_3(PO_4)_2$ can be described as purple but with a too large blue component (a*/b* ratio is too low to be adequate to use the pigment as primary magenta). For both the α-$NaCoPO_4$ and $LiCoPO_4$, three $Co^{2+}$ *d-d*

transitions are allowed and can be indexed using Tanabe-Sugano diagram for $d^7$ electronic configuration in octahedral coordination [42]–[45], $^4T_1$ (F)→ $^4T_1$ (P), $^4T_1$ (F)→ $^4A_2$ and $^4T_1$ (F)→ $^4T_2$. The first (high energy) transition is related with the absorption band in the visible range at about 550 nm, the second one merges in visible-NIR frontier near 750 nm and the last one (low energy) is located in the IR range at 1500 nm approximately. In comparison with $LiCoPO_4$, α-$NaCoPO_4$ is difficult to obtain without any traces of β-form. Consequently, the absorption bands are less intense and the purple color very less saturated. It was so decided to investigate substitutions in $LiCoPO_4$ framework.

Unit-cell parameters and atomic positions issued from our own structural refinement of the X-ray diffraction pattern of the as-prepared $LiCoPO_4$ compound (**Figure 2.a**), has allowed a representation of the structural network: the unit cell is represented along *b* and *c* axis projection (**Figures 2.b & 2.c**). $LiCoPO_4$ (orthorhombic system, Pnma space group) has an olivine type structure which consists of chains of octahedral sites with edge-sharing organization, along *b* axis, constituted alternatively of cobalt and lithium; the $P^{5+}$ ions are located in between these chains in isolated tetrahedral sites ([$PO_4$] oxo-anion groups). On the basis of rocksalt-type structure, lithium and cobalt ions occupy half of the octahedral sites, their Wyckoff positions are 4a and 4c, respectively and phosphorus occupies one eight of the tetrahedral positions. $CoO_6$ octahedral units are corner shared and cross-linked with the $PO_4$ tetrahedral, forming a three-dimensional network with tunnels that are occupied by Li ions along the (010) and (001) directions. The $CoO_6$ octahedron is highly distorted with 3 consecutive bonds with short length (2.06 Å- 2.11 Å), and the three opposite one's with long length (2.21 Å - 2.23 Å) (Fig. 2d). Thus, the cobalt octahedral sites exhibit a clear acentric character. This loss of centro-symmetry should be at the origin of the purple near magenta coloration of the $LiCoPO_4$ linked to the high intensity of the absorption bands. Clear differences appear in the 750 nm region corresponding to $^4T_1$ (F)→ $^4A_2$ electronic transition

and the distortion of polyhedral sites which strongly influence the color of the pigment. The lower intensity of this band observed for α-$NaCoPO_4$ can be attributed to the centrosymmetric character of the $Co^{2+}$ octahedral site (orthorhombic 2+2+2 with shorter at 1.98 Å, medium at 2.15 Å and longer at 2.36 Å bond lengths compared to $LiCoPO_4$) in agreement with the intensity of two others transitions. This band shift to higher wavelengths in the case of $Co_3(PO_4)_2$ because of the occurrence of various $Co^{2+}$ coordination number 5 and 6 with different crystal fields splitting.

### *3.2. $LiCo_xMg_{1-x}PO_4$ solid solution*

$LiCoPO_4$ powders, which are purple, represent a starting point, to obtain magenta inks. Doping with magnesium ion, *i.e.* replacing a part of $Co^{2+}$ ions with $Mg^{2+}$ ion has been attempted because: (i) The ionic radii are close: 0.72 Å and 0.745 Å in 6-coordinated site into oxides for $Mg^{2+}$ and $Co^{2+}$ ions, respectively, (ii) while the electronegativity of the magnesium ion is significantly lower than the one of cobalt ion, (iii) the $Mg^{2+}$ is not a chromophore ion, that means it does not produce a direct effect on the compound's color. Hence: (i) $LiCoPO_4$ and $LiMgPO_4$ can formed a complete solid solution, (ii) the ionic/covalence balance of metal-oxygen bonds are strongly impacted by the Mg to Co substitution, leading to a slight reduction of the octahedral distortion (less acentric sites with more 'isotropic $Mg^{2+}$') and a slight increase of crystal field splitting (bond distances decrease also observed by analyzing the Mg-O bond lengths in $LiMgPO_4$) around the cobalt chromophore ion and so to an ability to tune the coloration, (iii) the diffuse reflectance spectra and so the color of the compound is not polluted by new absorption bands.

The synthesis of $LiCo_xMg_{1-x}PO_4$ with x equal to 1; 0.7; 0.5; 0.3 and 0.2 has been performed by solid state route. The X-ray diffraction patterns of the as-prepared powders are reported in **Figure 3.a**. A single olivine phase (solid solution) is obtained for the whole range of compositions and no significant shift on the peak position is observed since the proximity of

$Mg^{2+}$ and $Co^{2+}$ ionic radii. In **Figure 3.b**, the UV-Vis-NIR absorbance curves (K-M transforms) are reported for comparison. All the spectra exhibit the three d-d transitions associated to cobalt(II) in octahedral site. Whatever the x magnesium concentration, the three allowed transitions, $^4T_1$ (F)→ $^4T_1$ (P), $^4T_1$ (F)→ $^4A_2$ and $^4T_1$ (F)→ $^4T_2$ remain located at 550 nm, 750 nm and 1500 nm, approximately. The main effect of the magnesium substitution is a continuous decrease of the cobalt absorption bands while the magnesium concentration increases. L*, a* and b* color parameters were extracted from diffuse reflectance curves, what allows, after L*a*b* → to RGB color space transformation, the representation of the color of each compound with any common software (**Figure 3.c**). Because of the absence of clear shift of the absorption bands, the hue parameters: a* and b* remain more or less constant regardless the doping rate. Moreover, the decrease of the K/S with the increase of magnesium rate induces a large growth of the luminosity parameter L*.

Finally, the substitution of cobalt by magnesium, despite the ionic/covalence balance of the metal-oxygen bonds as well as the $Co^{2+}$ octahedron distortion and crystal field splitting, leads to none significant change of the hue of $LiCo_xMg_{1-x}PO_4$ pigment in comparison with $LiCoPO_4$ pigment. Nevertheless, on the contrary to the hue parameters, the pigment luminosity can be easily controlled, in a large range raising from L*=33 for $LiCoPO_4$ up to L*=58 for $LiCo_{0.2}Mg_{0.8}PO_4$, with the change of the Mg/Co atomic ratio, opening interesting application for this solid solution as ceramic pigment.

### *3.3. $LiCo_{0.9}M_{0.1}PO_4$ solid solution with M =Mn, Cu, Ni or Fe.*

In this part, other chromophores ions (*3d* transition metals) have been used to substitute the cobalt: manganese, copper, nickel and iron, all with an oxidation number = + II, have been tested, with a molar concentration of 10 mol% ($LiCo_{0.9}M_{0.1}PO_4$ composition with M =Mn, Cu, Ni or Fe). XRD patterns of these compounds, reported in **Figure 4.a**. show that pure crystalline phase is detected whatever the M metal cation. As previously performed on the

$LiCo_xMg_{1-x}PO_4$ compounds, diffuse reflectance spectra are recorded and the experimental L*a*b* color parameters are extracted from these spectra (**Figures 4.b and 4.c**). All the absorbance spectra show the three d-d transitions associated to the cobalt ion, located at about 550 nm, 750 nm and 1500 nm. Manganese and iron ions do not impact the visible part of the diffuse reflectance spectra whereas one additional d-d transition is observed at 450 nm for the nickel-doped compound. One additional transition is located around 1000 nm for the copper-doped compound, *i.e.* in the near infrared range. The introduction of M cation also impacts the UV-visble frontier part of the diffuse reflectance spectrum. One should have to note the occurrence of O→M Charge Transfer Band especially for M= Fe, Cu. The $LiCo_{0.9}M_{0.1}PO_4$ compound with the maximal difference in comparison with the $LiCoPO_4$ reference is the nickel-substituted phosphate with the clear enhancement of the band around 750 nm ($^4T_1$ (F)→ $^4A_2$ transition) and in NIR region ($^4T_1$ (F)→ $^4T_2$ transition) whereas the intensity of $^4T_1$ (F)→ $^4T_1$ (P) transition centered at 550 nm remains identical. This large variation of peak intensity should be associated to the distortion of octahedral site as well as the appearance of d-d transitions associated to $Ni^{2+}$such as the band at 450 nm. Furthermore, the color of the $LiCo_{0.9}Ni_{0.1}PO_4$, is especially interesting with a redder hue than for the $LiCoPO_4$ reference: a*/b* ratio is decreased in a very significant way from -1.4 to -2.7 while nickel is partially substituted for cobalt in the solid solution. With the target to propose a facile access to a large color scale in view of pigment applications, the entire solid solution $LiCo_xNi_{1-x}PO_4$ has been explored.

### *3.4. $LiCo_xNi_{1-x}PO_4$ solid solution*

The X-ray diffraction patterns of the various $LiCo_xNi_{1-x}PO_4$ compounds, with x equal to 1; 0.9 ;0.8 ;0.7 ;0.5 ;0.2 and 0, are presented in **Figure 5.a**. A pure solid solution is obtained for the whole range of compositions. A shift of the diffraction peaks to a higher 2θ position can be observed with the decrease of the cobalt content. The *a*, *b* and *c* orthorhombic unit-cell

parameters, refined from the full pattern matching of the diffraction patterns using Fullprof software, are well governed by a linear Vegard's law, with a linear increase of both the parameters versus the cobalt concentration (**Figure 6**). This result is in good agreement with the $Ni^{2+}$ and $Co^{2+}$ ionic radii in octahedral coordination, equal to 0.69 Å and 0.745 Å, respectively. In more details, the observation of an isotropic effect of nickel to cobalt substitution on all the unit-cell parameters can be explained by the equivalent impact of an increase of the size of the $[CoO_6]$ octahedral sites in comparison of the $[NiO_6]$ octahedral sites, on all the *a*, *b* and *c* unit-cell parameters. Whatever, this clearly shows a solid solution is obtained whatever the x cobalt concentration in the $LiCo_{1-x}Ni_xPO_4$ composition series. UV-Vis-NIR absorbance spectra (KM transforms) are superimposed for the various as-prepared samples in **Figure 5.b**. In $LiCo_xNi_{1-x}PO_4$, there are two chromophores ions, $Ni^{2+}$ ($3d^8$) and $Co^{2+}$($3d^7$), both in octahedral coordination. Five pseudo-Gaussian bands are identified on the spectra. One can observe a large band in the NIR range (in between 1000 and 2250 nm) with an envelope shape which evolves versus the cobalt/nickel ratio. From Tanabe-Sugano diagrams [43] for $d^7$ (cobalt II) and $d^8$ (nickel II) electronic configuration, this large band is the superimposition of the $^4T_1$ (F) → $^4T_2$ : first allowed $d^7$ ($Co^{2+}$) transition and the $^3A_2$ → $^3T_2$: first allowed $d^8$ ($Ni^{2+}$) transition. In a same way, the second absorption band located at 800 nm is the superimposition of the $^4T_1$ (F) → $^4A_2$ : second allowed $d^7$ ($Co^{2+}$) transition and the $^3A_2$ → $^3T_1$: second allowed $d^8$ ($Ni^{2+}$) transition. The superimpositions (at least a partial overlapping) of the first absorption band and the second absorption band of nickel and cobalt into octahedral coordination must be discussed in further details. The two transition metals occupy the same crystallographic sites with almost identical crystal field splitting (10 Dq) but different B Racah parameters which depend on the nephelauxetic effect (the reduction of electrostatic interaction; then, comparable B values are expected for $Ni^{2+}$ and $Co^{2+}$ ions because of the almost identical electronegativity) induced by transition metals in the crystal

can vary from 870 $cm^{-1}$ (0.11 eV) to 1100 cm-1 (0.14 eV) for $Ni^{2+}$ and 780 $cm^{-1}$ (0.1 eV) to 1050 $cm^{-1}$ (0.13 eV) approximately for $Co^{2+}$ in octahedral coordination. The $B_{free}$ values for free $Co^{2+}$ and $Ni^{2+}$ ions are equal to 971 $cm^{-1}$ and 1041 $cm^{-1}$ respectively. The nephelauxetic effect is usually represented by the ratio $\beta = B/ B_{free}$. Then, the decrease of the Racah B parameter is due to the formation of covalent bond between transition metal and oxygen. Furthermore, in a first approximation taking into account the electronic configuration of these transition metals and the competition between the intra-atomic exchange energy (Hund rules) and the crystal field splitting, the following order 10Dq ($Ni^{2+}$) > 10 Dq ($Co^{2+}$) is expected. Indeed, from $d^7$ and $d^8$ electronic configuration, the first band energy (in eV) in NIR region is linked to the crystal field (10Dq in eV) and the *B* Racah parameter (eV) by a same equation (**equation 1**):

$$\frac{E}{B} = \frac{10Dq}{B} \qquad \textbf{Equation 1}$$

Whatever $Co^{2+}(3d^7)$ or $Ni^{2+}$ ($3d^8$) ions in a low crystal field and the second one in visible range around 750 nm is also described by the unique **equation 2**:

$$\frac{E}{B} = \frac{20Dq}{B} \qquad \textbf{Equation 2}$$

The equation 2 is fully valid for $Co^{2+}$ ($3d^7$) ion in low crystal field but consists in a good approximation in the case of $Ni^{2+}$ ions only for 10Dq /*B* << 10. From the evolution of the envelope shape (the enlargement of these bands is due to the LS-Russell Sanders coupling) of these two bands versus the cobalt/nickel ratio, the first energy band can be roughly located around 1600 nm and 1400 nm (near the peak/band with maximum intensity), for cobalt and nickel, respectively and the second energy band can be approximately positioned around 800 nm for both these transitions metals. Regarding the spectra of $LiCoPO_4$ and $LiNiPO_4$ extreme compounds, reported on **Figure 7**, and taking into account also the Tanabe-Sugano diagrams,

one can easily attribute, the third band at 430 nm to $Ni^{2+}$ ion in octahedral symmetry, corresponding to the ($\sigma 3$) $^4A_2 \rightarrow {}^3T_1$ (P) transition, and the band located at about 575 nm to $Co^{2+}$ ion in octahedral symmetry, corresponding to the ($\sigma 3$) $^3T_1$ (F) $\rightarrow {}^4T_1$ (P) transition, The main or most intense band/peak have been considered in a first approximation to estimate the third ($\sigma 3$) transition energy, reported on **Figure 7**. The two other one's, $\sigma 2$ and $\sigma 1$, represented also on **Figure 7** have been deduced from Tanabe-Sugano diagrams and are in the range of the previous values mentioned above. For $d^7$ and $d^8$ electronic configuration, from Tanabe Sugano diagrams, this third band can be approximated by the **equation 3a** and **equation 3b**, respectively.

$$\frac{E}{B} = 15 + \frac{\Delta}{B} \qquad \textbf{Equation 3a}$$

$$\frac{E}{B} = 15 + \frac{2\Delta}{B} \qquad \textbf{Equation 3b}$$

Hence, the third and last band positioning for the cobalt and nickel ions leads to estimate the crystal field splitting and Racah parameters around nickel and cobalt ions. Combining equation 1 and 3a, it comes $B(Co^{2+}) \cong 0.10$ eV (830 $cm^{-1}$) and then 10 Dq ($Co^{2+}$- Oh) ≅ 0.82 eV. According to the Tanabe-Sugano diagram for $d^8$ ion ($Ni^{2+}$), the B Racah parameter and 10Dq crystal field can be estimated and leads to $B(Ni^{2+}) \cong 0.11$ eV (900 $cm^{-1}$) and 10 Dq ($Ni^{2+}$- Oh) ≅ 0.90 eV in good agreement with the literature where crystal field splitting can vary between 0.8 and 1.3 eV for $Co^{2+}$ ions and between 0.9 and 1.5 eV for $Ni^{2+}$ ions in octahedral coordination. In this phosphate matrix, the crystal-field splitting is among the smallest one for these transition metals in octahedral symmetry in good agreement with the highly covalent character of $PO_4$ groups leading by competitive bonds to strong M-O (M=Co, Ni) ionic bonds with low crystal field. Furthermore, although nickel and cobalt are located in the same crystallographic site, a slightly higher crystal field splitting for $Ni^{2+}$ around 0.9 eV can be mentioned. A comparable B Racah parameter in comparison to $Co^{2+}$ ($\beta_{Co2+}$=

$B_{Co2+}/B_{free}$ = 0.85) ion in this phosphate, finally show the nephelauxetic effect is identical ($\beta_{Ni2+}$= $B_{Ni2+}/B_{free}$ = 0.86 = $\beta_{Co2+}$).

L*a*b* parameters and associated coloration are reported in **Figure 5.c**, for all the prepared $LiCo_xNi_{1-x}PO_4$ compounds. One can observe a very large color gradient from purple ($LiCoPO_4$) to yellow ($LiNiPO_4$). Indeed, even if two of the three absorption bands for nickel and cobalt are largely overlapped, the two low energy bands associated to the visible part of the spectrum are mainly governed by the third high-energy transition related to $Ni^{2+}$ and $Co^{2+}$ ions in octahedral sites which appear at different energies. Actually, the occurrence of a complete solid solution with $LiCo_xNi_{1-x}PO_4$ compositions and the evidence of two extreme compositions $LiCoPO_4$ and $LiNiPO_4$ with primer magenta and primer yellow color, respectively, leads to an access of a very large color scale, covering the yellow-orange-red-purple hues.

### *3.5. Extension to $LiCo_xMg_yNi_{1-(x+y)}PO_4$ solid solution*

"Quaternary" compounds can be imagined mixing in the same time nickel, cobalt and magnesium to obtain a tenability on both luminosity (L* parameter) and hue (a*-b* parameters) of the pigment. The color of all the as-prepared compounds are so depicted on one single ternary diagram where compounds could be written as $LiCo_xMg_yNi_{1-(x+y)}PO_4$, where x is the cobalt stoichiometry, y the magnesium stoichiometry and (1-(x+y)) the nickel stoichiometry (**Figure 8a**). A new compound with $LiCo_{0.4}Mg_{0.3}Ni_{0.3}PO_4$ composition (pigment K), *i.e.* near the center of such ternary diagram has been synthesized in order to illustrate how the chemical composition of this complex solid solution can be adjusted to tune the pigment color.

The panel of hues and luminosity obtained all along the study, in close relation with the pigment compositions, are all summarized in two schemes (**Figures 8.b** and **8.c**).

### *3.6. Pigments besides their application (about tinting strength, hiding power, etc.)*

In a final discussion, the pigment properties to take into account additionally to the colorimetric parameters (thermal stability, refractive index, hiding power and tinting strength) are discussed besides their application in electrophoretic inks, but also opening the discussion through various other potential applications.

The various pigment powders proposed in this paper have been synthetized at high temperature: 900°C, which is a thermal treatment not so far below the melting point of the prepared phosphates. Indeed, thermal treatment at 1100°C resulted to the compound melting. Moreover, for the use of such pigments in e.book inks, *i.e.* for a pigment referenced as Category C according to the Color Pigment manufactures association (CPMA): Category C deals with pigments suspended in liquid vehicles, [46], the thermal stability is highly satisfying, since e.inks are not submitted to temperatures above 100°C. With a thermal stability up to 1000°C, our pigments are also perfectly adequate for a use as suspended in plastics and other polymers which require only moderate heat stability (category B), and even, they can be used for coloring ceramic glazes with the requirement of a low refractory character for the glassy matrix (category A).

The tinting strength has been estimated. Pigments have been mixed with two different white powders which have different refractive index ($TiO_2$ n= 2.61 and $CaCO_3$ n=1.63). The diffuse reflectance of mixtures made from the white powder and our pigment, with 50 wt% of $LiCo_xNi_{1-x}PO_4$ (x=0 ,1 or 0.5), have been recorded. Diffuse reflectance spectra of the mixtures and evolution of the optical contrast between the as-prepared mixtures and the white pigment as reference are presented in **Figure 9.** This optical contrast (norm of the vector in % between the coordinates of the white reference and the pigment mixtures, both in L*a*b* space, considering the norm of the vector between the coordinates of the white reference and the pure pigment, both in L*a*b* space, is 100%) is used as a direct quantifcation of the pigment tinting strength. First, one can be see that the reflectance curve of the mixtures is roughly

intermediate in comparison with the one of the $LiCo_xNi_{1-x}PO_4$ compounds (named A for $LiCoPO_4$, B for $LiCo_{0.5}Ni_{0.5}PO_4$ and C for $LiNiPO_4$) and those of $TiO_2$ (E) and $CaCO_3$ (D). The calculation of the white / pigment mixtures optical contrasts are in the range 42-50% using the calcium carbonate as white reference and in the range 20-30% using titanium dioxide as white reference. Hence, the tinting strength of our phosphate pigments can be roughly estimated as the one of the calcium carbonate (but far below the one of titanium dioxide). Using the Glastone Dale equation (**equation 4**), refractive index of $LiCo_xNi_{1-x}PO_4$ compound have been calculated:

$$n = 1 + \rho(LiCoPO_4).\sum \rho i.ki \qquad \textbf{Equation 4}$$

Where, ρ is the density of the complex oxide and the terms ρi and ki are the density and the refractive coefficient of each oxide respectively. For $LiCo_xNi_{1-x}PO_4$ compound, a refractive index of 1.775 is obtained. This refractive index is similar to the refractory index of $CaCO_3$ but lower than the one of $TiO_2$, in perfect agreement with our tinting strength evaluation. Finally, the hiding powder of our pigment besides the requirements of the final electrophoretic inks, is quite difficult to evaluate. This hiding power shows positive correlation besides the increase of refractive index (which exhibits a value comparable to the one of the calcium carbonates, *i.e.* compatible with their use in electrophoretic inks), the increase of the pigment volume fraction inside the ink, the decrease of the particle sizes after the pigment dispersion into the organic medium (both these parameters being link with the pigment scattering power).

## 4. CONCLUSION

By exploring phosphate series, it is worth noting that the well-known olivine $LiCoPO_4$ compound exhibits a frank purple color, near primary magenta: a Holy Graal for inorganic

pigments. The luminosity of the magenta can be changed without modifying too much the hue thanks to a magnesium to cobalt substitution by preparing the complete $LiCo_xMg_{1-x}PO_4$ solid solution characterized by XRD and optical absorbance. $LiNiPO_4$, which is isostructural to $LiCoPO_4$ and $LiMgPO_4$, exhibits a frank yellow color, near a primary yellow. A large color scale can so be reached from basic formulation mixing nickel and cobalt ions in the desired proportion to form the $LiCo_xNi_{1-x}PO_4$ solid solution: yellow-orange-red-purple colors can so be obtained. Furthermore, the attribution of d-d transitions in the whole Visible-NIR range of the optical absorbance spectra of $LiCo_xNi_{1-x}PO_4$ solid solution allows determining in a first approximation the crystal field splitting and the B Racah parameter. Then even if $Ni^{2+}$ and $Co^{2+}$ cations occupy the same crystallographic sites, the crystal field splitting remains slightly higher for $Ni^{2+}$, but rather low around 0.8-0.9 eV whereas the $\beta = B_{Ni2+}/B_{free} = B_{Co2+}/B_{free}$ covalency parameter are identical for both these transition metals in this phosphate matrix. The obtaining of two of the three subtractive model's colors with inorganic pigment opens large applications. Indeed, these pigments, once modified would allow to obtain hybrid particles, electrically charged and dispersed in organic media. The refractive index of the as-prepared pigment panels (about 1.8), lead to a tinting strength and so a hiding power comaprable with calcium carbonate (which is a white pigment with very large application as for the whitening of commercial papers). Thus, these as-prepared pigments would permit colored electrophoretic inks formulation, that could be used in color electrophoretic image displays, *i.e.* the target is to use these pigments as the coloring mater of the next e-book (e-readers) generation.

**FIGURES:**

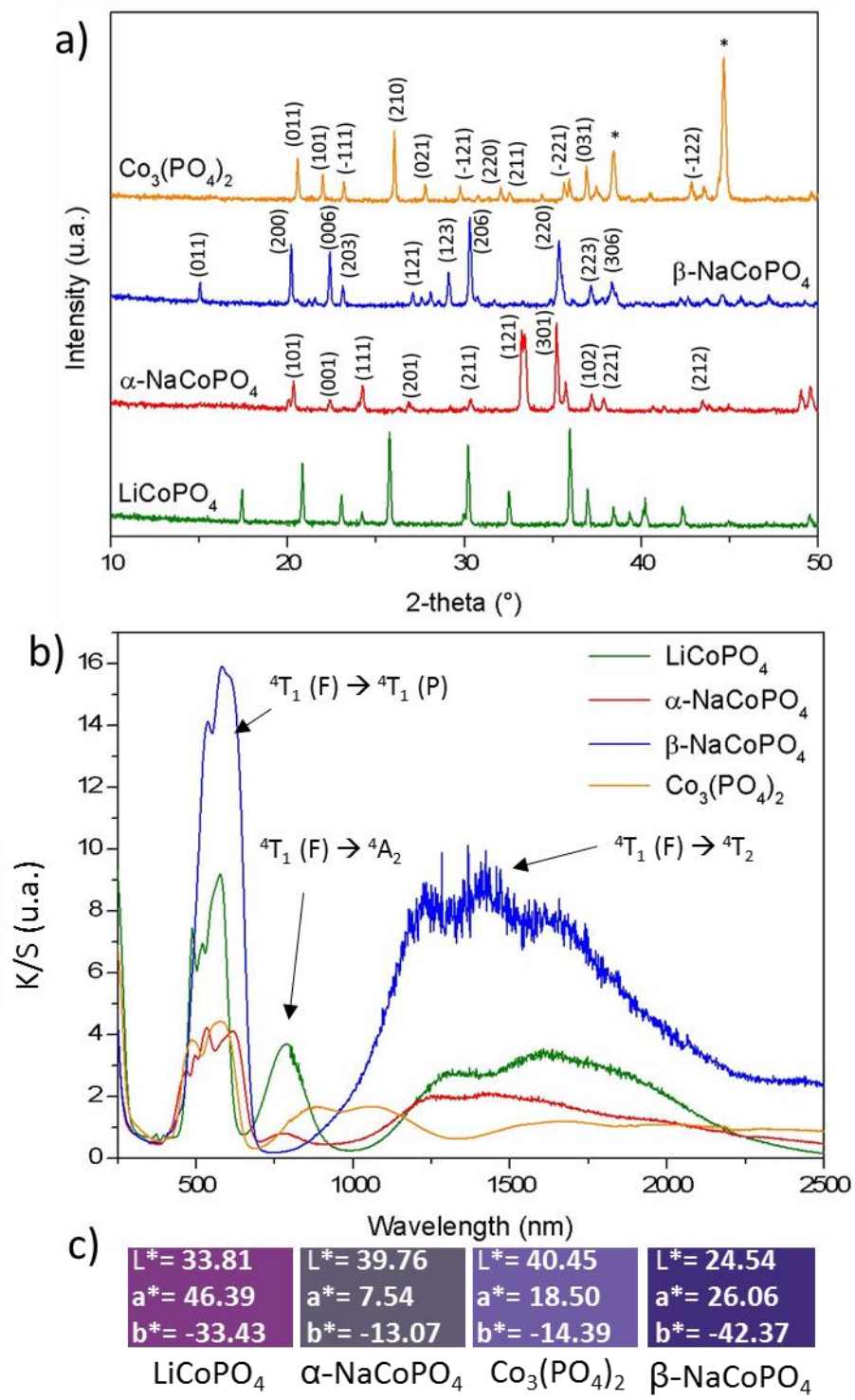


**Figure 1. a)** XRD patterns (* Al support), **b)** K/S spectra and **c)** L*a*b* colour parameters of $Co_3(PO4)_2$, $NaCoPO_4$ and $LiCoPO_4$ compounds prepared from solid state route at 900 °C.

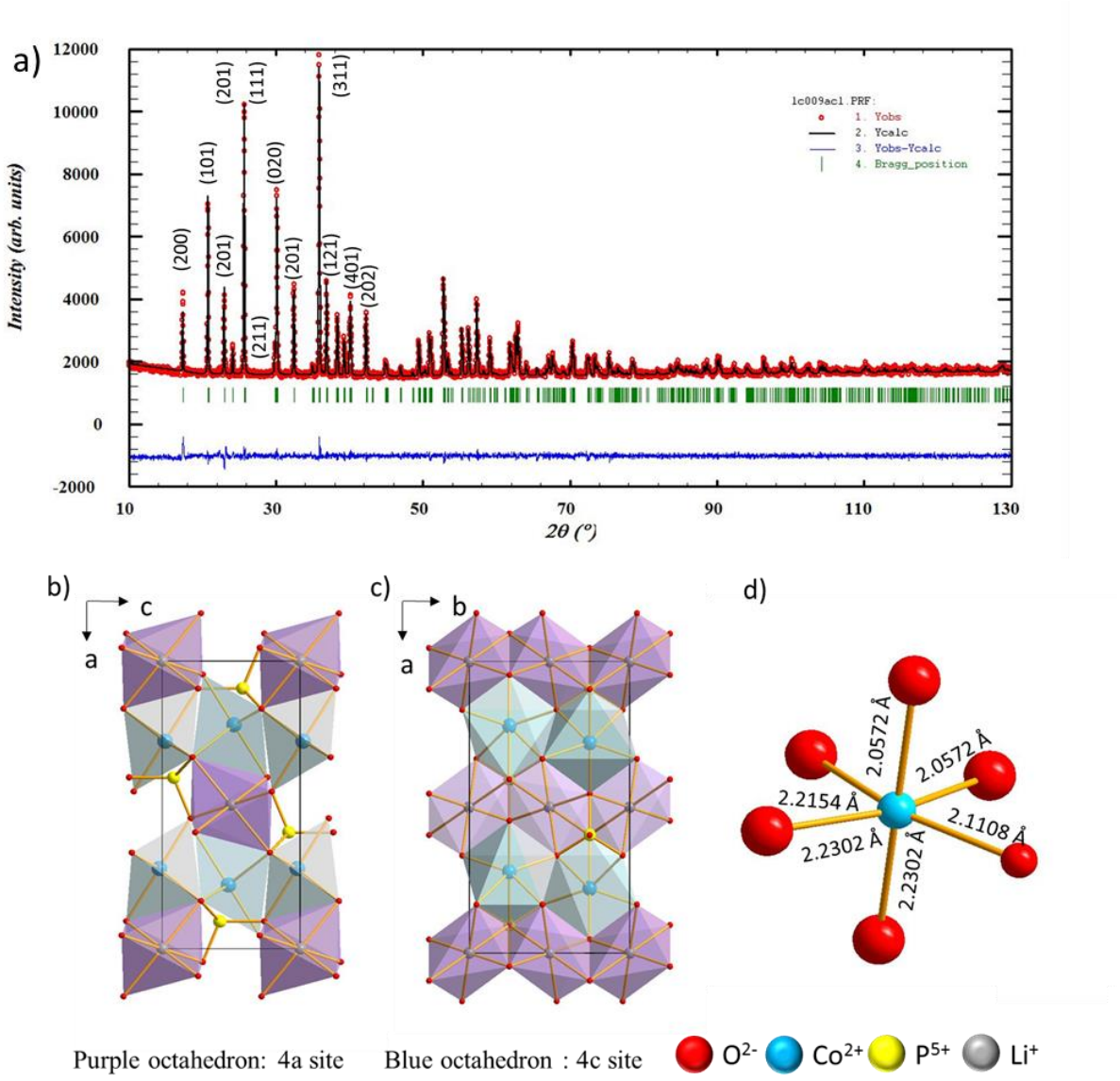


**Figure 2. a) and b)** Representation of the $LiCoPO_4$ compound from parameter extracted with Rietveld refinement. **c)** Distorted octahedron of the cobalt in 4c site.

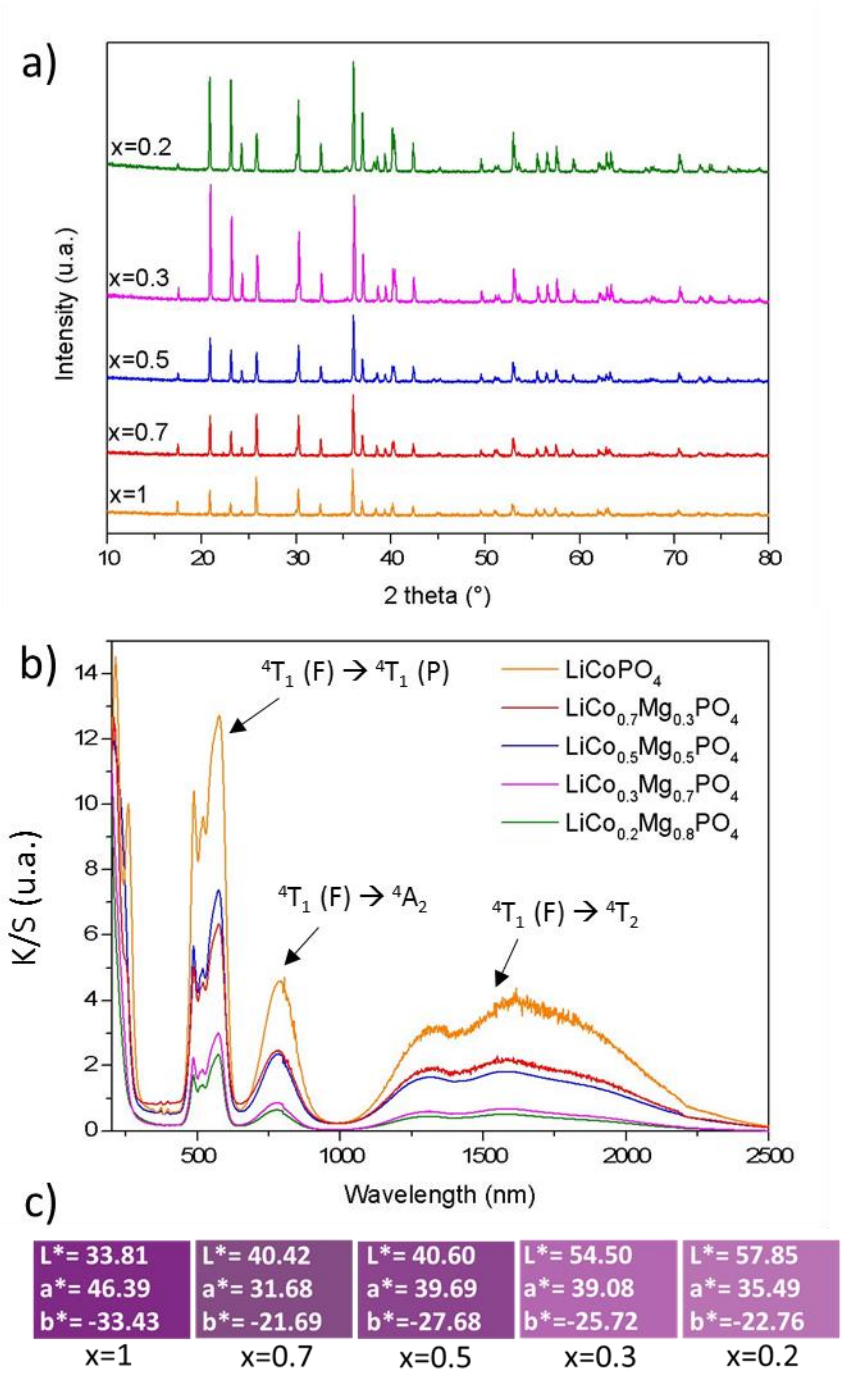


**Figure 3. a)** XRD patterns, **b)** K/S spectra and **c)** L*a*b* colour parameters of $LiCo_xMg_{1-x}PO_4$ (x= 1; 0.7; 0.5; 0.3 and 0.2) compounds prepared from solid state route at 900 °C.

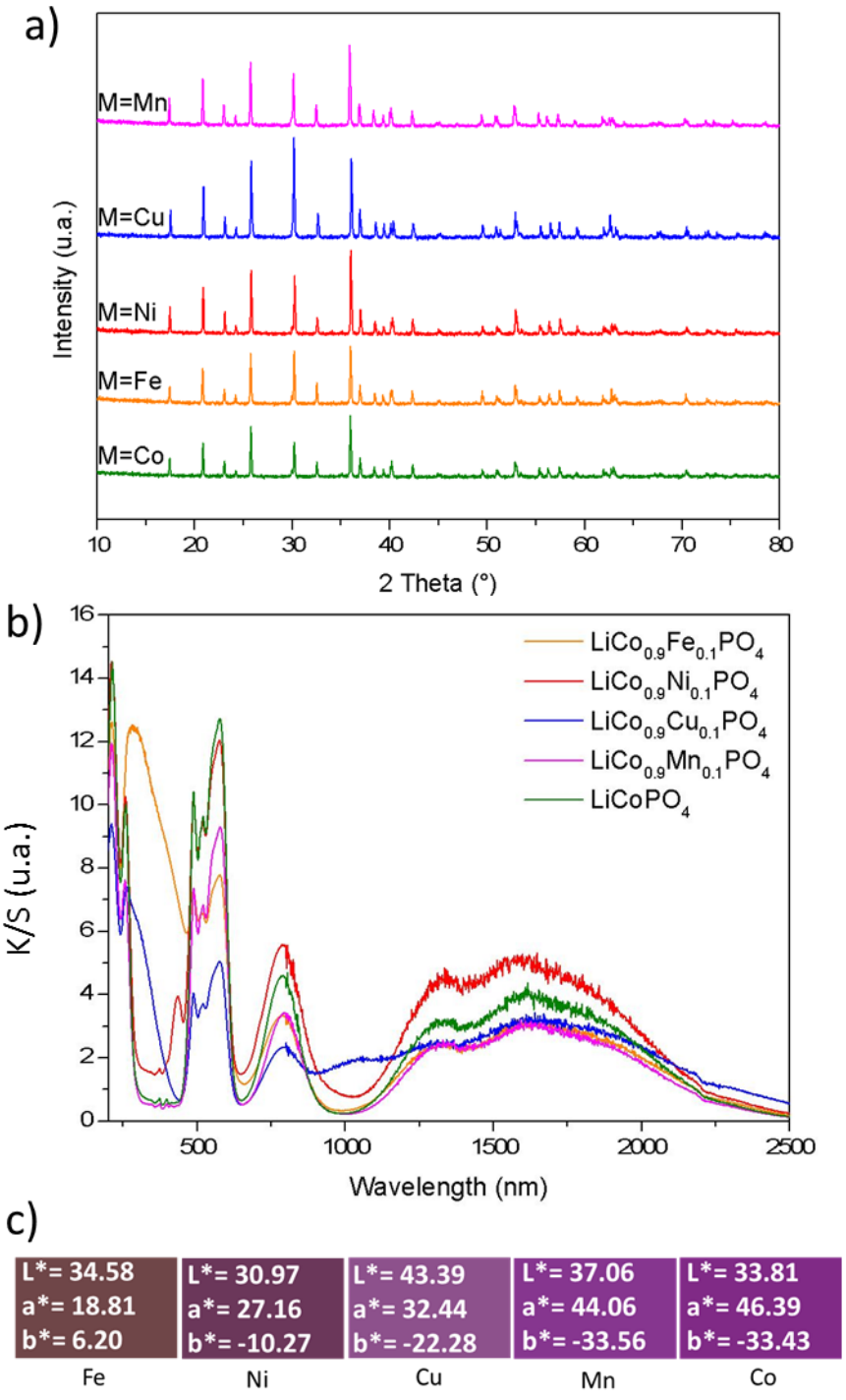


**Figure 4. a)** XRD patterns, **b)** K/S spectra and **c)** L*a*b* colour parameters of $LiCo_xM_{1-x}PO_4$ (M= Fe, Ni, Cu, Mn and Co) compounds prepared from solid state route at 900 °C.

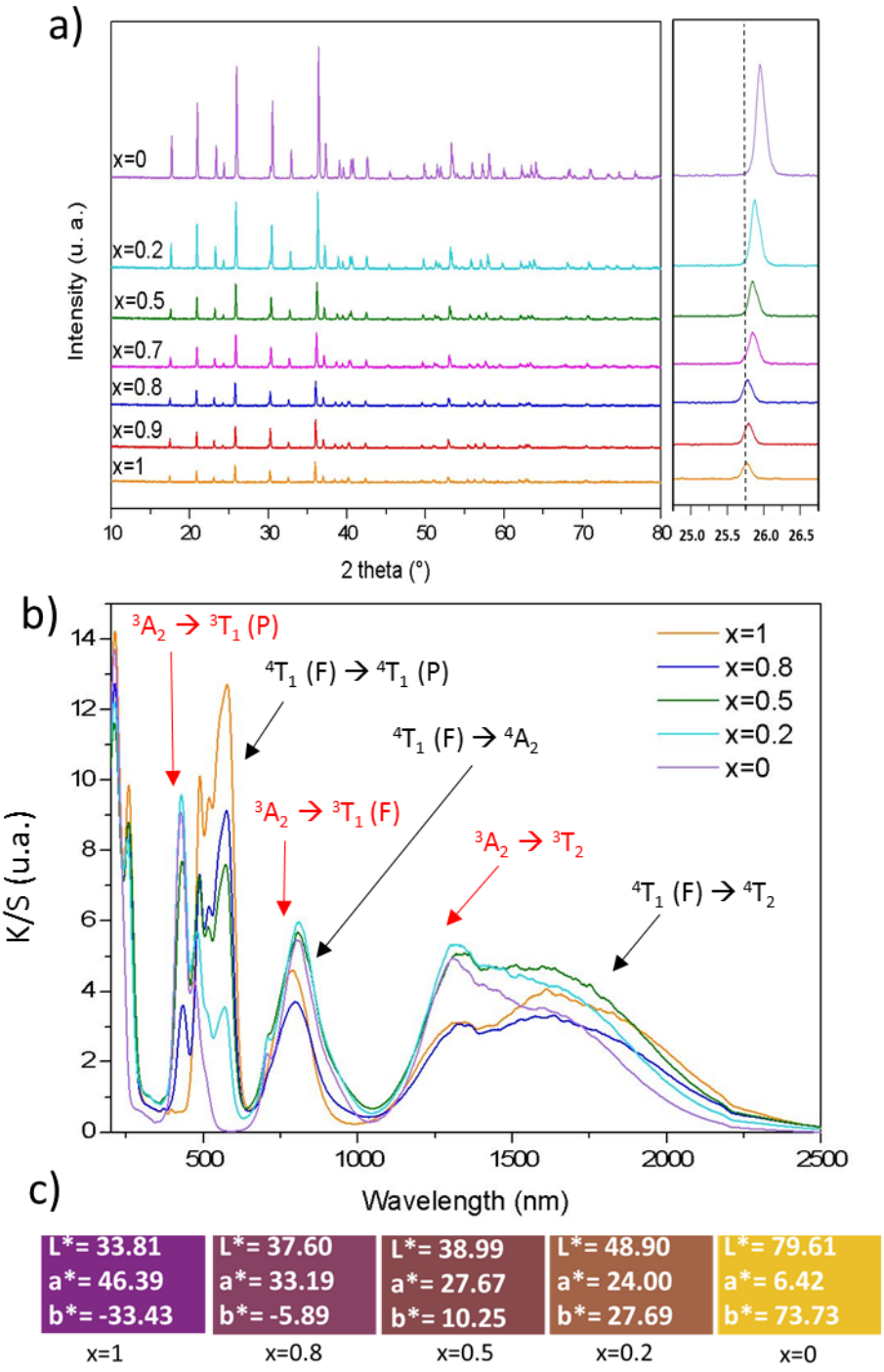


**Figure 5. a)** XRD patterns, **b)** K/S spectra with $Co^{2+}$ and $Ni^{2+}$ spectroscopic transitions which are in black and red, respectively and **c)** L*a*b* colour parameters of $LiCo_xNi_{1-x}PO_4$ (x= 1; 0.9; 0.8; 0.7; 0.5; 0.2 and 0) compounds prepared from solid state route at 900 °C.

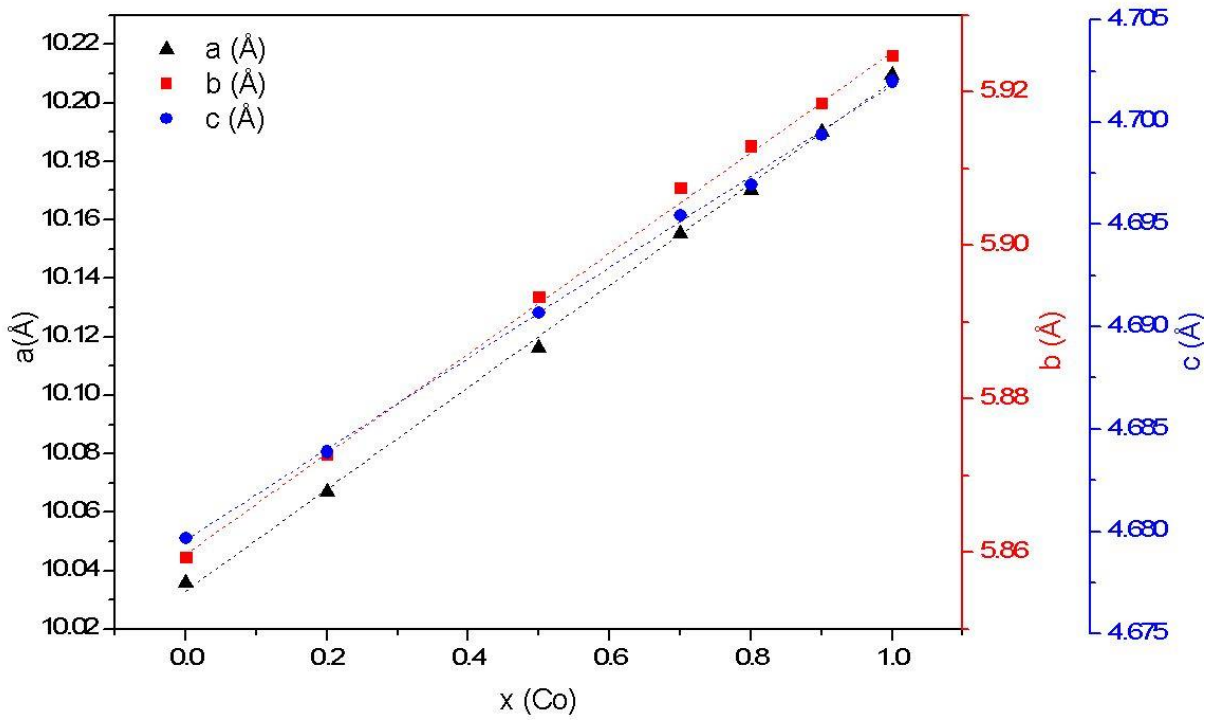


**Figure 6.** Evolution of unit cell dimensions a, b and c with the cobalt rate in the $LiCo_xNi_{1-x}PO_4$ solid solution.

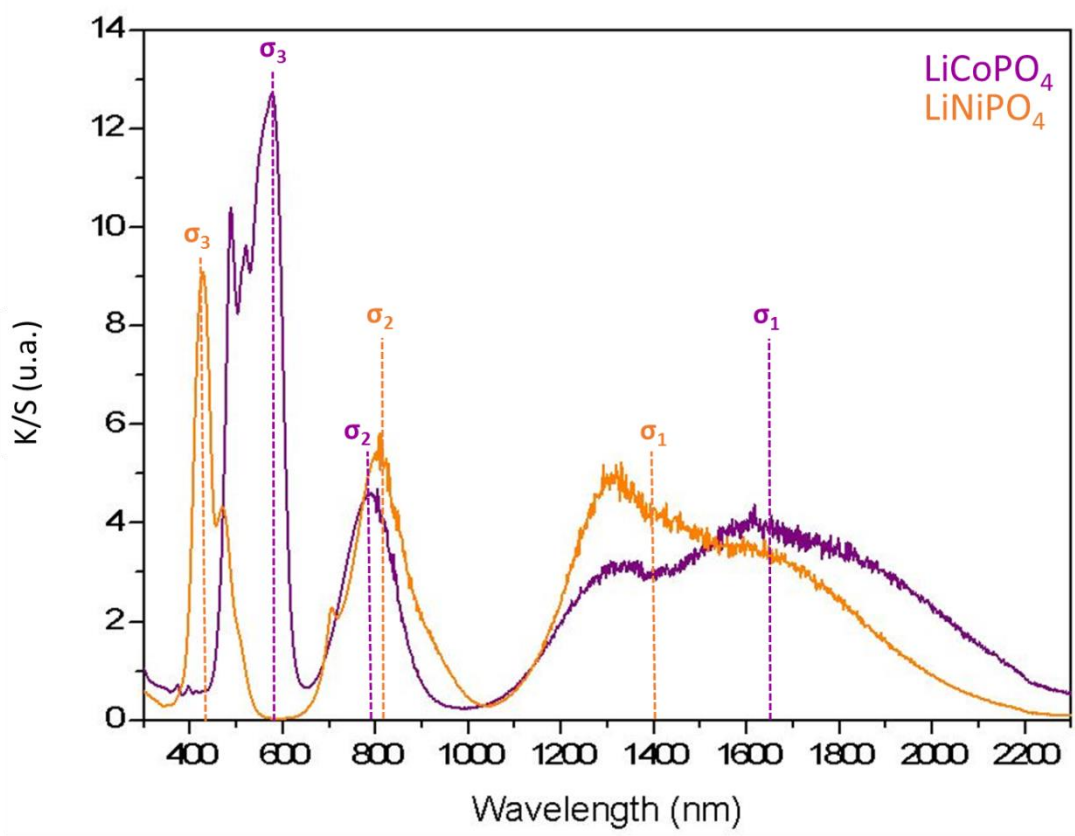


| Ion | B ($cm^{-1}$) | Dq (eV) ($cm^{-1}$) | $\sigma_1$ ($cm^{-1}$) | $\sigma_2$ ($cm^{-1}$) | $\sigma_3$ ($cm^{-1}$) |
|---|---|---|---|---|---|
| $Co^{2+}$ | 830 | 0.82 (6614) | 6060 $^4T_1\,(F) \rightarrow {}^4T_2$ | 12658 $^4T_1\,(F) \rightarrow {}^4A_2$ | 17391 $^4T_1\,(F) \rightarrow {}^4T_1\,(P)$ |
| $Ni^{2+}$ | 900 | 0.90 (7259) | 7071 $^3A_2\,(F) \rightarrow {}^3T_2$ | 12214 $^3A_2\,(F) \rightarrow {}^3T_1\,(F)$ | 23142 $^3A_2\,(F) \rightarrow {}^3T_1\,(P)$ |

**Figure 7** : K/S spectra of $LiCoPO_4$ and $LiNiPO_4$ phases with the three σ1, σ2 and σ3 various electronic transitions attributed on the basis of Tanabe Sugano diagrams. The deduced B Racah parameters and 10Dq crystal field splitting associated to $Co^{2+}$ and $Ni^{2+}$ in these phosphates as well as the three transitions energies are reported in the table below.

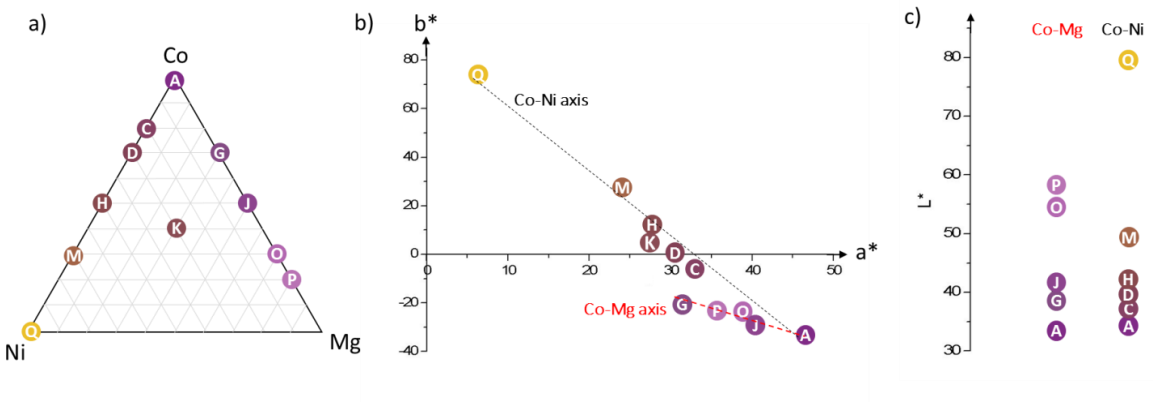


**Figure 8. a)** Ternary colored diagram **b)** Evolution of the chromatic parameters a* and b* **c)** Evolution of the lightness parameter for the $LiCo_xMg_yNi_{1-(x+y)}PO_4$ compounds.

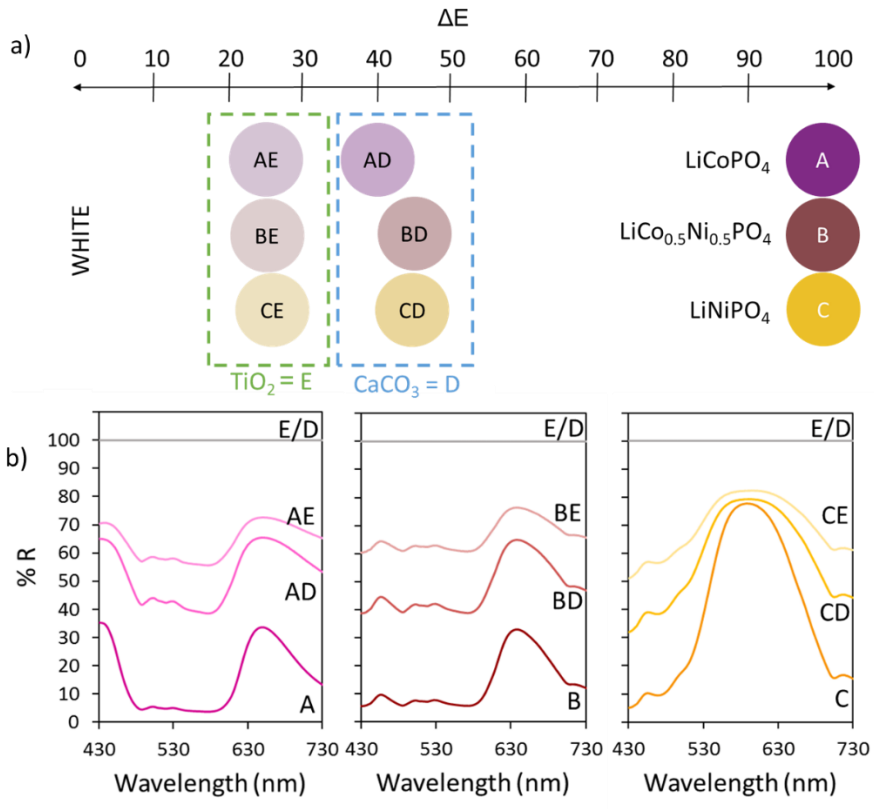


**Figure 9. a)** Evolution of the optical contrast **b)** Diffuse reflectance spectra of $LiCo_xNi_{1-x}PO_4$ (x=1,0.5 and 0) powders and of mixtures with 50%w. of $CaCO_3$ or $TiO_2$ and $LiCo_xNi_{1-x}PO_4$ compounds.

AUTHOR INFORMATION

## Corresponding Author

# Corresponding author: manuel.gaudon@icmcb.cnrs.fr

## Author Contributions

The manuscript was written through contributions of all authors. All authors have given approval to the final version of the manuscript. ‡These authors contributed equally.

## Notes

Any additional relevant notes should be placed here.

REFERENCES


[1] A. Clearfield and D.S. Thakur, “Zirconium and titanium phosphates catalysts: a review”, *Appl. Catal.*, vol. 26, pp. 1-26, 1986.

[2] M. Conte *et al.*, “Chemically Induced Fast Solid-State transitions of w-VOPO4 in Vanadium Phosphate Catalysts,” *Science*, vol. 313, no. 5791, pp. 1270–1273, 2006.

[3] M. W. Kanan and D. G. Nocera, “In situ formation of an oxygen-evolving catalyst in neutral water containing phosphate and Co2+,” *Science*, vol. 321, no. 5892, pp. 1072–1075, 2008.

[4] A. Clearfield, “Role of ion exchange in solid-state chemistry,” *Chem. Rev.*, vol. 88, no. 1, pp. 125–148, 1988.

[5] S. T. Wilson, B. M. Lok, C. A. Messina, T. R. Cannan, and E. M. Flanigen, “Aluminophosphate molecular sieves: A new class of microporous crystalline inorganic solid,” *J. Am. Chem. Soc.*, vol. 104, no. 4, pp. 1145–1146, 1982.

[6] A. Bhaumik and S. Inagaki, “Mesoporous Titanium Phosphate Molecular Sieves with Ion-Exchange Capacity,” *J. Am. Chem. Soc.*, vol. 123, no. 4, pp. 691–696, Jan. 2001.

[7] M. E. Hagerman and K. R. Poeppelmeier, “Review of the Structure and processing-Defect-property Relationships of Potassium Titanyl Phosphate: A Strategy for Novel Thin-Film photonic Devices.,” *Chem. Mater.*, vol. 7, pp. 602–621, 1995.

[8] R. K. Brow, “the structure of simple phosphate glasses,” *J. Non-Cryst. Solids*, vol. 263, pp. 1–28, 2000.

[9] M. S. Whittingham, “Lithium Batteries and Cathode Materials,” *Chem. Rev.*, vol. 104, no. 10, pp. 4271–4302, Oct. 2004.

[10] C. Delmas, “The nasicon- type titanium phosphate ATi2(PO4)3(A=Li,Na) as electrode materials,” *Solid State Ion.*, vol. 28–30, pp. 419–423, 1988.

[11] G. Monros, “Pigment, Ceramic,” in *Encyclopedia of Color Science and Technology*, R. Luo, Ed. New York, NY: Springer New York, 2013, pp. 1–15.

[12] R. . Eppler, “Colorants for Ceramics,” *Kirk-Othmer Encycl. Chem. Technol.*, 2013.

[13] A. K. Cheetham, G. Ferey, and T. Loiseau, “Open-Framework Inorganic Materials,” *Angew. Chem. Int. Ed.*, vol. 38, pp. 3268–3292, 1999.

[14] C. Ding, A. Han, M. Ye, Y. Zhang, L. Yao, and J. Yang, “Hydrothermal synthesis and characterization of novel yellow pigments based on $V^{5+}$ doped $BiPO_4$ with high near-infrared reflectance,” *RSC Adv.*, vol. 8, no. 35, pp. 19690–19700, 2018.

[15] T. K. Ghorai, D. Dhak, A. Azizan, and P. Pramanik, “Investigation of phase formation temperature of nano-sized solid solution of copper/cobalt molybdate and chromium–phosphate (M1xCr1−xMoxP1−xO4) [M1=Co, Cu],” *Mater. Sci. Eng. B*, vol. 121, no. 3, pp. 216–223, Aug. 2005.

[16] R. El ouenzerfi *et al.*, “Relationships between structural and luminescence properties in Eu3+ doped oxyphosphate silicate apatite,” *Opt. Mater.*, vol. 16, pp. 301–310, 2001.

[17] N. Clavier, N. Dacheux, P. Martinez, V. Brandel, R. Podor, and P. Le Coustumer, “Synthesis and characterization of low-temperature precursors of thorium–uranium (IV) phosphate–diphosphate solid solutions,” *J. Nucl. Mater.*, vol. 335, no. 3, pp. 397–409, Dec. 2004.

[18] S. N. Achary, O. D. Jayakumar, A. K. Tyagi, and S. K. Kulshresththa, “Preparation, phase transition and thermal expansion studies on low-cristobalite type Al1−xGaxPO4 (x=0.0, 0.20, 0.50, 0.80 and 1.00),” *J. Solid State Chem.*, vol. 176, no. 1, pp. 37–46, Nov. 2003.

[19] A. A. Belik, A. P. Malakho, B. I. Lazoryak, and S. S. Khasanov, “Synthesis and X-ray Powder Diffraction Study of New Phosphates in the Cu3(PO4)2–Sr3(PO4)2 System: Sr1.9Cu4.1(PO4)4, Sr3Cu3(PO4)4, Sr2Cu(PO4)2, and Sr9.1Cu1.4(PO4)7,” *J. Solid State Chem.*, vol. 163, no. 1, pp. 121–131, Jan. 2002.

[20] B. Comiskey, J. . Albert, H. Yoshizawa, and J. Jacobson, “An electrophoretic ink for all-printed reflective electronic displays,” *Nature*, vol. 394, no. 6690, pp. 253–255, 1998.

[21] J. A. Rogers and Z. Bao, “Printed plastic electronics and paperlike displays,” *J. Polym. Sci. Part Polym. Chem.*, vol. 40, no. 20, pp. 3327–3334, Oct. 2002.

[22] C. A. Kim *et al.*, “Microcapsules as an electronic ink to fabricate color electrophoretic displays,” *Synth. Met.*, vol. 151, no. 3, pp. 181–185, Aug. 2005.

[23] M. Badila, A. Hébraud, C. Brochon, and G. Hadziioannou, “Design of Colored Multilayered Electrophoretic Particles for Electronic Inks,” *ACS Appl. Mater. Interfaces*, vol. 3, no. 9, pp. 3602–3610, Sep. 2011.
[24] D.-G. Yu *et al.*, “Preparation and characterization of titanium dioxide core/polymer shell hybrid composite particles prepared by emulsion polymerization,” *J. Appl. Polym. Sci.*, vol. 92, no. 5, pp. 2970–2975, 2004.
[25] Y. Fang, J. Wang, L. Li, Z. Liu, P. Jin, and C. Tang, “Preparation of chromatic composite hollow nanoparticles containing mixed metal oxides for full-color electrophoretic displays,” *J. Mater. Chem. C*, vol. 4, no. 24, pp. 5664–5670, 2016.
[26] B. Peng *et al.*, “Monodisperse light color nanoparticle ink toward chromatic electrophoretic displays,” *Nanoscale*, vol. 8, no. 21, pp. 10917–10921, 2016.
[27] C. Jablonski, G. Grundler, U. Pieles, S. Stebler, R. Oehrlein, and Z. Szamel, “Synthesis and Electrophoretic Properties of Novel Nanoparticles for Colored Electronic Ink and e-Paper Applications,” *Chim. Int. J. Chem.*, vol. 70, no. 5, pp. 366–368, May 2016.
[28] S. Tamilarasan, M. L. P. Reddy, S. Natarajan, and J. Gopalakrishnan, “Developing Intense Blue and Magenta Colors in α-LiZnBO3: The Role of 3d-Metal Substitution and Coordination,” *Chem. - Asian J.*, vol. 11, no. 22, pp. 3234–3240, Nov. 2016.
[29] M. Llusar, A. Forés, J. A. Badenes, J. Calbo, M. A. Tena, and G. Monrós, “Colour analysis of some cobalt blue pigments,” *J. Eur. Ceram. Soc.*, vol. 21, pp. 1121–1130, 2001.
[30] R. Galindo, M. Llusar, M. A. Tena, G. Monrós, and J. A. Badenes, “New pink ceramic pigment based on chromium (IV)-doped lutetium gallium garnet,” *J. Eur. Ceram. Soc.*, vol. 27, no. 1, pp. 199–205, Jan. 2007.
[31] A. Fernández-Osorio, E. Pineda-Villanueva, and J. Chávez-Fernández, “Synthesis of nanosized (Zn1−xCox)Al2O4 spinels: New pink ceramic pigments,” *Mater. Res. Bull.*, vol. 47, no. 2, pp. 445–452, Feb. 2012.
[32] N. Gorodylova, V. Kosinová, Ž. Dohnalová, P. Bělina, and P. Šulcová, “New purple-blue ceramic pigments based on CoZr4(PO4)6,” *Dyes Pigments*, vol. 98, no. 3, pp. 393–404, Sep. 2013.
[33] N. Gorodylova, V. Kosinová, Ž. Dohnalová, P. Šulcová, and P. Bělina, “A comparative study of the influence of mineralisers on the properties of CoZr4(PO4)6-based pigments,” *Dyes Pigments*, vol. 111, pp. 156–161, Dec. 2014.
[34] L. Shengyi, L. Yingchun, Z. Rongbo, L. Hongguang, and D. Wensi, “Study on Co-KZr2(PO4)3-Type Crystalline Purple Ceramic Pigments,” *Appl. Mech. Mater.*, vol. 34–35, pp. 790–794, 2010.
[35] N. Pailhé, M. Gaudon, and A. Demourgues, “(Ca2+, V5+) co-doped Y2Ti2O7 yellow pigment,” *Mater. Res. Bull.*, vol. 44, no. 8, pp. 1771–1777, Aug. 2009.
[36] N. Imanaka, T. Masui, and M. Itaya, “Synthesis of an environmentally friendly and nontoxic new pigment based on rare earth phosphate,” *Chem. Lett.*, vol. 32, no. 4, pp. 400–401, 2003.
[37] A. El Jazouli, B. Tbib, A. Demourgues, and M. Gaudon, “Structure and colour of diphosphate pigments with square pyramid environment around chromophore ions (Co2+, Ni2+, Cu2+),” *Dyes Pigments*, vol. 104, pp. 67–74, May 2014.
[38] M. Müller-Sommer, R. Hock, and A. Kirfel, “Rietveld refinement study of the cation distribution in (Co, Mg)-olivine solid solution,” *Phys. Chem. Miner.*, vol. 24, no. 1, pp. 17–23, 1997.
[39] L. A. Frolova and A. V. Derimova, “Formation and the colour development in nanocrystalline CoZn phosphate,” in *2017 IEEE International Young Scientists Forum on Applied Physics and Engineering (YSF)*, 2017, pp. 335–338.
[40] P. Feng, X. Bu, and G. D. Stucky, “Synthesis and characterizations of a polymorphic sodium cobalt phosphate with edge-sharing Co2+ octahedral chains,” *J. Solid State Chem.*, vol. 131, no. 1, pp. 160–166, 1997.
[41] C. Jähne, C. Neef, C. Koo, H.-P. Meyer, and R. Klingeler, “A new LiCoPO4 polymorph via low temperature synthesis,” *J. Mater. Chem. A*, vol. 1, no. 8, p. 2856, 2013.
[42] Y. Tanabe and S. Sugano, “On the absorption spectra of complex ions I,” *J. Phys. Soc. Jpn.*, vol. 9, no. 5, pp. 753–766, 1954.
[43] Y. Tanabe and S. Sugano, “On the absorption spectra of complex ions II,” *J. Phys. Soc. Jpn.*, vol. 9, no. 5, pp. 766–779, 1954.

[44] Y. Tanabe and S. Sugano, “On the absorption spectra of complex ions III,” *J. Phys. Soc. Jpn.*, vol. 11, no. 8, pp. 864–877, 1956.
[45] Y. Tanabe and H. Kamimura, “On the absorption spectra of complex ions IV,” *J. Phys. Soc. Jpn.*, vol. 13, no. 4, pp. 394–411, 1958.
[46] “CPMA Classification and Chemical Description of the Complex Inorganic Color Pigments, Fourth Edition.” Complex Inorganic Color Pigments Committee, Color Pigments Manufacturers Association, Inc., 2013.

**For Table Of Content only**

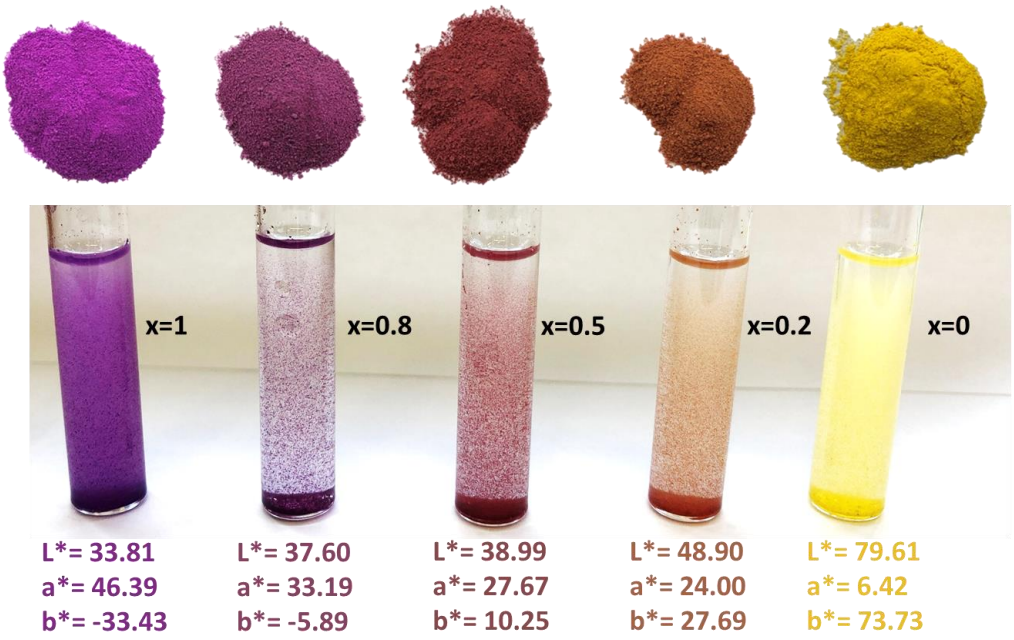


**TOC Synopsis**

A single solid solution ($LiMPO_4$ with M a transition metal: nickel or cobalt) leads to a pigment series showing purple (magenta) to yellow through orange, red colorations.